Digital Discovery

ROYAL SOCIETY OF CHEMISTRY

PAPER

View Article Online
View Journal

Cite this: DOI: 10.1039/d5dd00585j

Artificial intelligence-driven optimization of closed-loop CO_2 capture and conversion

Yongwook Kim, [a] Basil M. W. de Hepcée, [b] Mehrdad Mokhtari,[a] Marzieh Namdari,[a] Giuseppe V. Crescenzo[a] and Curtis P. Berlinguette *[abcd]

Received 24th December 2025
Accepted 31st May 2026

DOI: 10.1039/d5dd00585j

rsc.li/digitaldiscovery

Reactive carbon capture couples CO_2 capture with electrochemical CO_2 upgrading. A major advantage of reactive carbon capture is that CO_2 can be released from a liquid sorbent without the need for heat or vacuum. However, it is challenging to find conditions capable of both capturing and upgrading CO_2 effectively. The capture of CO_2 requires the sorbent to be at a high pH, while CO_2 electrolysis is more effective at a lower pH. In this study, we used an artificial intelligence (AI)-driven strategy to optimize several operating variables for reactive carbon capture. The optimization yielded increases in CO_2 capture efficiency from 30% to 83% and faradaic efficiency for CO (FE_{CO}) from 30% to 42%. These new benchmarks lead to a CO breakeven price of <$1 per kilogram for reactive carbon capture, a value that represents one of the lowest cost pathways for converting air into fuel.

Introduction

Carbon capture and utilization involves at least three key steps: (i) capturing waste CO_2 using a sorbent; (ii) recovering the captured CO_2 from the sorbent; and (iii) upgrading the captured CO_2 into value-added fuels and chemicals.[1–7] The final step of upgrading the captured CO_2 can be performed in an electrolyzer.[8–13] However, the second step of recovering the captured CO_2 from a capture solution, followed by purifying and pressurizing the captured CO_2, must occur outside the electrolyzer. The heat or vacuum needed to recover the captured CO_2 is both capital- and energy-intensive.[14]

Reactive carbon capture integrates CO_2 capture with conversion to bypass these energy-intensive steps.[14,15] A key advantage of reactive carbon capture is that electricity can be used to release the captured CO_2 from the capture solution rather than heat or vacuum.[16,17] This feature is beneficial as renewable electricity is less carbon-intensive.[18] Reactive carbon capture also enables the electrolyzers to be fed with liquids instead of pressurized CO_2 gas.[14,15] The use of liquid feedstock makes the electrolyzer easier to build and operate, as well as less sensitive to $O_{2(g)}$ and SO_x impurities during operation.[19,20]

For example, consider direct air capture using alkaline solutions (enriched in OH^- or CO_3^{2-}) to capture CO_2.[5] The eluent from the CO_2 capture unit, also known as "reactive carbon solution", can be fed into a "reactive carbon electrolyzer" to simultaneously liberate and upgrade CO_2 from the capture solution. At the same time, the reactive carbon electrolyzer can create an alkaline eluent that can be recycled back into the CO_2 capture unit for further carbon capture (Fig. 1). A reactive carbon electrolyzer generates acid equivalents that react with (bi)carbonate ions in the reactive carbon solution to generate high concentrations of CO_2 *in situ* (eqn (1)). This *in situ* generated CO_2 ("*i*-CO_2") is then electrochemically reduced into carbon-containing products such as carbon monoxide (CO; eqn (2)).[16,17,21–25] The byproduct of this CO_2 reduction reaction (CO_2RR) is OH^- (eqn (2)), which is recycled to capture CO_2 from flue gas or air (eqn (3)). We recently coupled a reactive carbon electrolyzer with a CO_2 capture unit to demonstrate continuous, closed-loop CO_2 capture and conversion.[26]

$$HCO_{3(aq)}^- + H_{(aq)}^+ \leftrightharpoons i\text{-}CO_{2(g)} + H_2O_{(l)} \quad (1)$$

$$i\text{-}CO_{2(g)} + H_2O_{(l)} + 2\,e^- \rightarrow CO_{(g)} + 2OH_{(aq)}^- \quad (2)$$

$$CO_{2(g)} + OH_{(aq)}^- \leftrightharpoons HCO_{3(aq)}^- \quad (3)$$

For this closed-loop reactive carbon capture process to be practical, the capture solution that exits the electrolyzer and enters the CO_2 capture unit must be at a high pH to capture CO_2 effectively. However, the reactive carbon electrolyzer works more effectively at a low pH. This tension can be addressed by changing a range of parameters, such as the size and capture solution characteristics of the CO_2 capture unit or the size and operating parameters of the reactive carbon electrolyzer.[27] The

[a]Department of Chemistry, University of British Columbia, 2036 Main Mall, Vancouver, British Columbia V6T 1Z1, Canada. E-mail: cberling@chem.ubc.ca
[b]Department of Chemical and Biological Engineering, University of British Columbia, 2360 East Mall, Vancouver, British Columbia V6T 1Z3, Canada
[c]Stewart Blusson Quantum Matter Institute, University of British Columbia, 2355 East Mall, Vancouver, British Columbia V6T 1Z4, Canada
[d]Canadian Institute for Advanced Research (CIFAR), 661 University Avenue, Toronto, Ontario, M5G 1M1, Canada

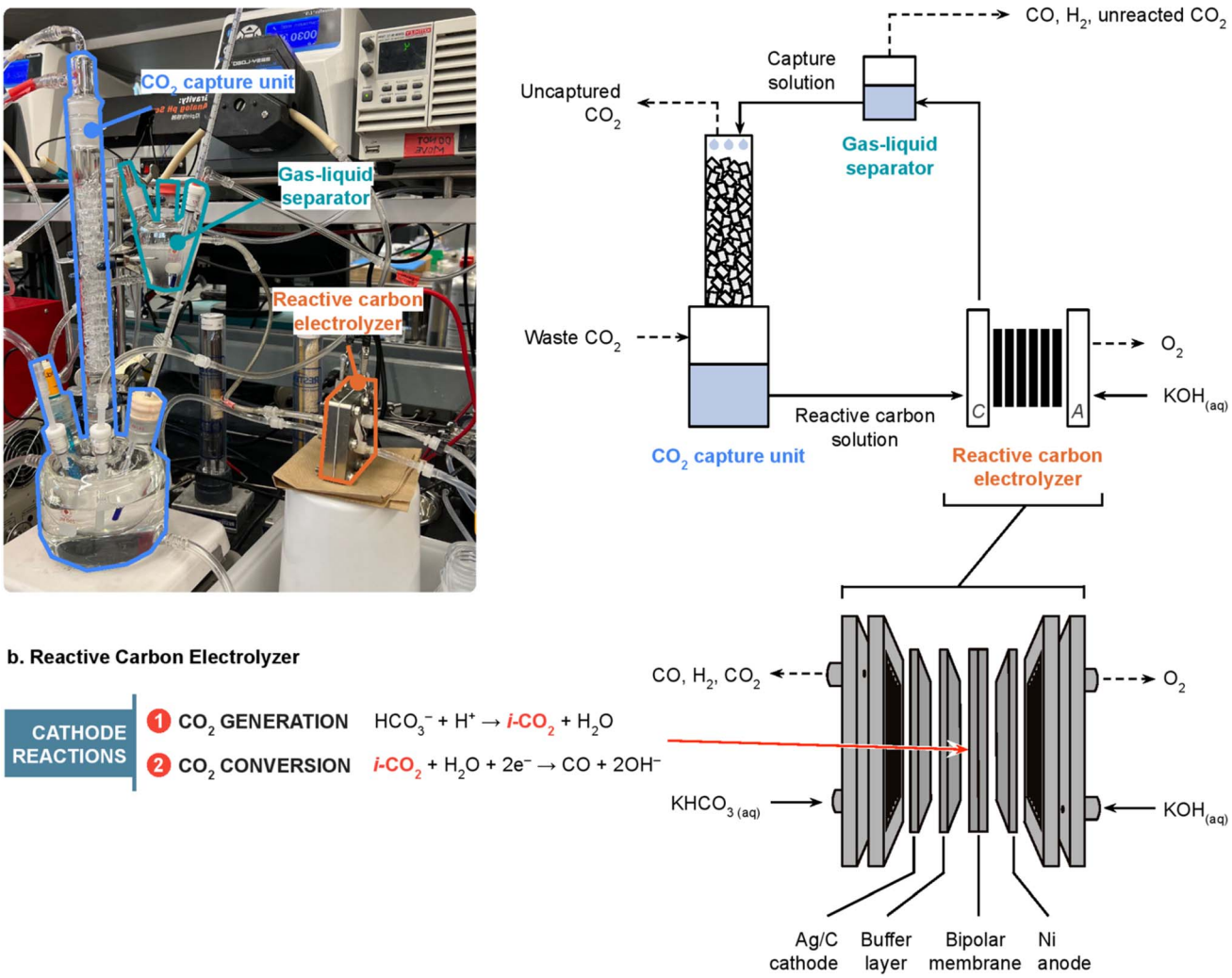

Fig. 1 A reactive carbon capture system. (a) A photograph and schematic of the reactive carbon capture system. The system includes three main components: a CO_2 capture unit (blue), a reactive carbon electrolyzer (orange), and a gas–liquid separator (teal). The schematic highlights the flow of liquids (solid lines) and gasses (dashed lines) within the system. In the CO_2 capture unit, a "capture solution" enriched with hydroxide/carbonate ions reacts with CO_2 to form a "reactive carbon solution" rich in (bi)carbonate ions. This reactive carbon solution is fed into the reactive carbon electrolyzer, where CO is produced alongside hydroxide ions as a byproduct. The hydroxide ions regenerate the alkalinity of the solution, forming a capture solution that is recycled back to the CO_2 capture unit. (b) Components of the reactive carbon electrolyzer and the reactions occurring within the electrolyzer. In the cathode chamber, H^+ ions electrochemically generated by the bipolar membrane react with (bi) carbonate ions to produce CO_2 *in situ* ("*i*-CO_2"). This *i*-CO_2 is then electrochemically upgraded to CO. For simplicity, the reaction of carbonate ions with H^+ is omitted. A hydrophilic and uncatalyzed "buffer layer" was placed between the membrane and cathode to mitigate the highly acidic environment and suppress the hydrogen evolution reaction. A 1 M KOH solution is supplied to the anode compartment. A bipolar membrane separates the cathode and anode chambers.

evaluation of these parameters creates a massive parameter space to test and optimize. For example, testing combinations of just four operating parameters (*e.g.*, temperature and flow rate of the reactive carbon solution, flow rate of the simulated flue gas, and current density of the electrolyzer), each at 15 different values, could take decades to execute experimentally (SI Note 1).

To accelerate the optimization of a reactive carbon capture system, we implemented artificial intelligence (AI) to identify the Pareto surface that considers CO_2 capture efficiency of the CO_2 capture unit and the selectivity of the reactive carbon electrolyzers for converting CO_2 into CO (*i.e.*, the faradaic efficiency, FE_{CO}).[28,29] Here, we show that multi-objective Bayesian optimization successfully identified conditions for closed-loop reactive carbon capture that achieve a CO_2 capture efficiency of 83% and a FE_{CO} of 42% using a simulated flue gas containing 15% CO_2 (balance N_2). These values are a significant improvement from the previous benchmarks of a CO_2 capture efficiency of 30% and a FE_{CO} of 30%.[26] The improvement in performance metrics corresponds to a breakeven price for CO production of

$0.86 per kg, with the reactive carbon electrolyzer operating at a current density of 234 mA cm^{-2} and a cell voltage of 4.8 V. Consequently, this work presents an economically viable pathway for CO_2 capture and conversion.

Experimental

Raw materials

K_2CO_3 (ACS reagent, ≥99.0%, Sigma Aldrich, USA), KOH (ACS reagent, ≥85%, pellets, Sigma Aldrich, USA), ethylenediaminetetraacetic acid (EDTA; 99%, Sigma Aldrich, USA), silver nanoparticles (<100 nm particle size, contains PVP as dispersant, 99.5% trace metals basis, Sigma Aldrich, USA), glycine (ReagentPlus®, ≥99% (HPLC), Sigma Aldrich, USA), and Mixed Cellulose Ester (MCE) Membrane Filters (8.0 μm Pore Size, Sigma Aldrich, USA) were purchased and used as received. Fumasep® FBM bipolar membranes (BPMs), Freudenberg H23 carbon paper, and Nafion® D2020 (20 wt% in a mixture of lower aliphatic alcohols and water) were purchased from Fuel Cell Store, USA. Nickel foam anodes were purchased from MTI Corporation, USA.

Materials preparation

Nickel foam anodes were cut to 2.5 × 2.5 cm and used as received without any modification. Cathodes were prepared by spray-coating silver nanoparticles onto carbon paper. The cathode catalyst ink was prepared by mixing 27 mg of silver nanoparticles (<100 nm) with 10 μL of 20 wt% Nafion® (Nafion Dispersion D2020) in 9 mL of ethanol, and the catalyst ink was sonicated for 20 min for even dispersion. Carbon paper was cut into 2.5 × 2.5 cm pieces. The cathode catalyst ink was then deposited onto these pieces of carbon paper using an airbrush until the catalyst loading reached 2 mg cm^{-2} (gravimetric measurement). The air pressure for the airbrush was set to 20 psi. The hotplate below the cathode samples was heated to 150 °C to accelerate solvent evaporation during the spray-coating process. A BPM was cut into a larger area of 5 × 5 cm to accommodate sealing and was used as is. The hydrophilic, uncatalyzed "buffer layer" (*e.g.*, mixed cellulose ester membrane filters with 8.0 μm pore size) was also cut to 2.5 × 2.5 cm and placed between the BPM and the cathode.

Reactive carbon electrolyzer design and assembly

The reactive carbon electrolyzer comprises flow plates with serpentine flow patterns that sandwich the membrane electrode assembly (MEA). The cathode and anode flow plates were both made of grade 3 titanium. The MEA consists of a nickel foam anode, a carbon paper cathode spray-coated with silver nanoparticles with a buffer layer (*e.g.*, mixed cellulose ester membrane filters with 8.0 μm pore size), and a BPM separating the anode and cathode chambers. The BPM was configured in reverse bias, meaning the cation exchange layer faces the cathode and the anion exchange layer faces the anode. The active area is 2.24 × 2.24 cm, which equates to a geometric surface area of 5 cm^2. This geometric surface area was used to calculate the current density reported in this work. All the assembly components were pressed against each other with no gap ("zero-gap architecture"). The assembly was tightened with 8 bolts of 6.35 mm diameter to a torque of 3 N m.

CO_2 capture unit design

A lab-scale CO_2 capture unit was assembled using glass components sourced from commercial vendors. This design was guided by previous findings, which showed that stainless steel and brass materials in the CO_2 capture unit negatively affected the performance of reactive carbon capture.[26] The CO_2 capture unit consists of two main stages: (i) a jacketed flask (6959-48, Ace Glass) that serves as a reservoir for excess liquid capture solution. The water jacket enables temperature control of the capture solution, and (ii) a column (6573-04, Ace Glass) with a height of 20.3 cm that houses the packing materials. The column has a perforated glass disc at the bottom to support the packing materials while allowing liquid and gas flow between the reservoir and the packed column. The column is filled with glass Raschig rings (8033-04, Ace Glass) measuring 5 mm in diameter and 5 mm in height. The Raschig rings were randomly loaded into the packed column, forming a packed bed with a height of 17 cm. The top of the column was sealed with a vacuum take-off adapter (5193-08, Ace Glass).

The capture solution exits the CO_2 capture unit from the reservoir and enters the CO_2 capture unit from the top of the packed column through the vacuum take-off adapter. The gas enters the CO_2 capture unit at the overhead of the reservoir and exits at the gas outlet at the top of the packed column.

Gas–liquid separator design

The gas–liquid separator was created by modifying a tapered flask (9473-24, Ace Glass) obtained from a commercial vendor. The modification involved adding inlet and outlet ports on the flask body to accommodate the liquid flow.

Experimental procedure for reactive carbon capture

The reactive carbon capture setup consists of three main components: a CO_2 capture unit, a reactive carbon electrolyzer, and the gas–liquid separator described above (Fig. 1a). The components are interconnected as follows: the liquid outlet of the CO_2 capture unit is connected to the cathode liquid inlet of the reactive carbon electrolyzer, the cathode liquid outlet of the reactive carbon electrolyzer is connected to the liquid inlet of the gas–liquid separator, and the liquid outlet of the gas–liquid separator is connected back to the liquid inlet of the CO_2 capture unit.

To ensure continuous circulation of the capture solution, two peristaltic pumps were installed (each with a pump motor (07522-20, Masterflex L/S) and a pump head (77200-62, Masterflex L/S)). One pump delivers the solution from the liquid outlet of the CO_2 capture unit to the cathode liquid inlet of the reactive carbon electrolyzer, while the other delivers the capture solution from the liquid outlet of the gas–liquid separator and the liquid inlet of the CO_2 capture unit.

A capture solution was prepared by dissolving 34.5 g of K_2CO_3, 1.46 g of EDTA, and 1.875 g of glycine in 250 mL of

deionized water, yielding a solution with concentrations of 1 M K_2CO_3, 20 mM EDTA, and 0.1 M glycine. EDTA was added to the 1 M K_2CO_3 solution to prevent electrolyte impurities from electrodepositing onto the electrode surface, while glycine was included to increase CO_2 capture kinetics.

The 1 M K_2CO_3 solution with 0.1 M glycine and 20 mM EDTA was circulated during all experiments at flow rates determined by an artificial intelligence algorithm. A constant 175 sccm flow of N_2 purged the headspace of the gas–liquid separator, carrying electrolysis products to the gas chromatograph (GC; SRI-8610C, SRI Instruments, USA). Simulated flue gas containing 15% CO_2 and 85% N_2 entered the CO_2 capture unit from the bottom at fixed flow rates set by mass flow controllers and exited at the top. The flow rates were determined by an artificial intelligence algorithm. 500 mL of 1 M KOH solution was circulated through the anode chamber at a flow rate of 100 mL min^{-1} using a peristaltic pump (9154K53, McMaster-Carr, USA).

Two-electrode electrolysis experiments were conducted at ambient pressure with a custom-designed zero-cap electrolyzer using a power supply (2260B-30-72 720W, Keithley Instruments, USA). Current density is expressed as the total current applied divided by the geometric surface area of the electrodes (*e.g.*, 5 cm^2).

Product analysis

The composition of the gaseous products from the gas–liquid separator was analyzed with a GC at different time lengths. The GC was equipped with a packed MolSieve 5 Å column and a packed HaySep D column. Argon (Praxair, 99.999%) was used as the carrier gas. A flame ionization detector (FID) with a methanizer was used to quantify reduced carbon products (*e.g.*, CO, CH_4, C_2H_4, C_2H_6, and C_3H_8) and CO_2. A thermal conductivity detector (TCD) was used to quantify H_2. The GC was calibrated by injecting different calibration gas mixtures from NorLAB containing CO, CO_2, H_2, CH_4, C_2H_6, and C_3H_8 at concentrations ranging from 100–50,000 ppm for each gas (balance N_2).

The faradaic efficiency (FE_i) was calculated based on gas concentrations obtained from GC analyses using Faraday's law of electrolysis:

$$FE_i = \frac{x_i z_i n F}{I} \quad (4)$$

where z_i is the number of electrons transferred per mole of gaseous product i involved in the reduction reaction, F is Faraday's constant, x_i is the mole fraction of gaseous product i in the gaseous mixture analyzed using GC, n is the molar flow rate, and I is the total applied current. The molar flow rate was derived from the volumetric flow rate using the ideal gas law.

The molar flow rate of *in situ* generated CO_2 ($n_{i\text{-}CO_2}$) was calculated by adding the molar flow rates of unreacted CO_2 ($n_{CO_2,out}$) and CO product ($n_{CO,out}$) exiting the reactive carbon electrolyzer. We assumed that CO was the only reduced carbon product in this study:

$$n_{i\text{-}CO_2} = n_{CO_2,out} + n_{CO} \quad (5)$$

Results and discussion

Reactive carbon capture system

The reactive carbon capture system used in our investigation consists of a benchtop CO_2 capture unit, a reactive carbon electrolyzer, and a gas–liquid separator (Fig. 1). In the CO_2 capture unit, an alkaline CO_2 capture solution reacts with CO_2 from simulated flue gas to form a (bi)carbonate-enriched reactive carbon solution. This solution is fed into the electrolyzer, where *i*-CO_2 is generated (eqn (1)) and subsequently reduced to CO (eqn (2)) within the same electrolyzer. The gas–liquid separator, which is a sealed reservoir, isolates the gaseous products exiting the electrolyzer so that the gaseous products can be measured with gas chromatography. The only detected products were CO, H_2, and unreacted CO_2. The liquid outlet of the CO_2 capture unit connects to the inlet of the cathode chamber of the electrolyzer, while the cathode outlet connects to the liquid inlet of the gas–liquid separator. The liquid outlet of the gas–liquid separator is cycled back to the liquid inlet of the CO_2 capture unit, which forms a closed-loop for liquid recirculation.

A BPM separates the electrolyzer anode and cathode chambers (Fig. 1). The anode chamber is fed with 1 M KOH electrolyte and mediates the oxygen evolution reaction at a porous nickel anode. The cathode chamber is fed with the reactive carbon solution from the CO_2 capture unit and mediates the CO_2RR using a silver nanoparticle catalyst spray-coated onto carbon paper. A hydrophilic, uncatalyzed "buffer layer" (*e.g.*, mixed cellulose ester membrane filter) is placed between the membrane and cathode to mitigate the highly acidic environment and suppress the hydrogen evolution reaction.[30] The Experimental Section provides full details of the electrolyzer design and components.

The initial reactive carbon capture experiment used a 1 M K_2CO_3 capture solution containing 0.1 M glycine and 20 mM ethylenediaminetetraacetic acid (EDTA). Glycine was added to increase CO_2 capture rates without impacting FE_{CO}.[26] We selected a concentration of 0.1 M because this concentration increases CO_2 capture efficiency while minimizing any decrease in FE_{CO}.[26] EDTA (20 mM) was added as a chelating agent to prevent electrolyte impurities from depositing onto the cathode surface.[31] We previously identified 20 mM as the minimum concentration needed to effectively suppress metal impurity deposition. The addition of EDTA slightly decreased the rate of CO_2 capture, but it had no effect on the FE_{CO} (Fig. S1). The capture solution was circulated at a flow rate of 30 mL min^{-1} through the reactive carbon capture system. We used simulated flue gas (15% CO_2, 85% N_2) as a waste CO_2 source, and it was fed to the CO_2 capture unit at a flow rate of 235 sccm. The electrolyzer was operated at a constant current density of 188 mA cm^{-2}. The initial operating conditions were determined using Latin hypercube sampling with random selection (see Table S1).

Performance metrics for reactive carbon capture

We then set out to quantify the CO_2 capture efficiency and FE_{CO} after the reactive carbon solution reached a steady-state pH. We

assume that a steady-state pH occurs when the CO_2 capture rate in the CO_2 capture unit and the CO_2 conversion rate in the reactive carbon electrolyzer are balanced (Fig. 2). These performance metrics (CO_2 capture efficiency and FE_{CO}) demonstrate the capacity of our system to capture and convert CO_2 into value-added products, emphasizing the importance of optimizing both capture and conversion conditions.

The CO_2 capture efficiency quantifies the ability of the CO_2 capture unit to capture CO_2 from the simulated flue gas. We define this metric as the ratio of the molar flow rate of captured carbon ($n_{carbon,out}$) to the molar flow rate of CO_2 entering the capture unit ($n_{carbon,in}$). Under steady-state conditions, the molar flow rate of captured carbon encompasses the molar flow rates of both unreacted CO_2 ($n_{CO_2,out}$) and produced CO ($n_{CO,out}$) in the electrolyzer. Put differently, $n_{carbon,out}$ equals the molar flow rate of *i*-CO_2 ($n_{i\text{-}CO_2}$) generated within the reactive carbon electrolyzer under steady-state conditions. However, when the system is not at steady-state, the equilibrium reaction expressed in eqn (3) causes a portion of the captured CO_2 to remain in the reactive carbon solution. Thus $n_{carbon,out}$ does not equate to $n_{i\text{-}CO_2}$.

The value of FE_{CO} indicates what fraction of the current provided to the electrolyzer is directed toward CO production. This metric quantifies how efficient the system is at converting captured CO_2 to CO.

AI-guided reactive carbon capture

After our initial experiment, we used Bayesian optimization to manipulate four key operating variables (Fig. S2): (i) temperature and (ii) flow rate of the reactive carbon solution; (iii) flow rate of the simulated flue gas; and (iv) the current density

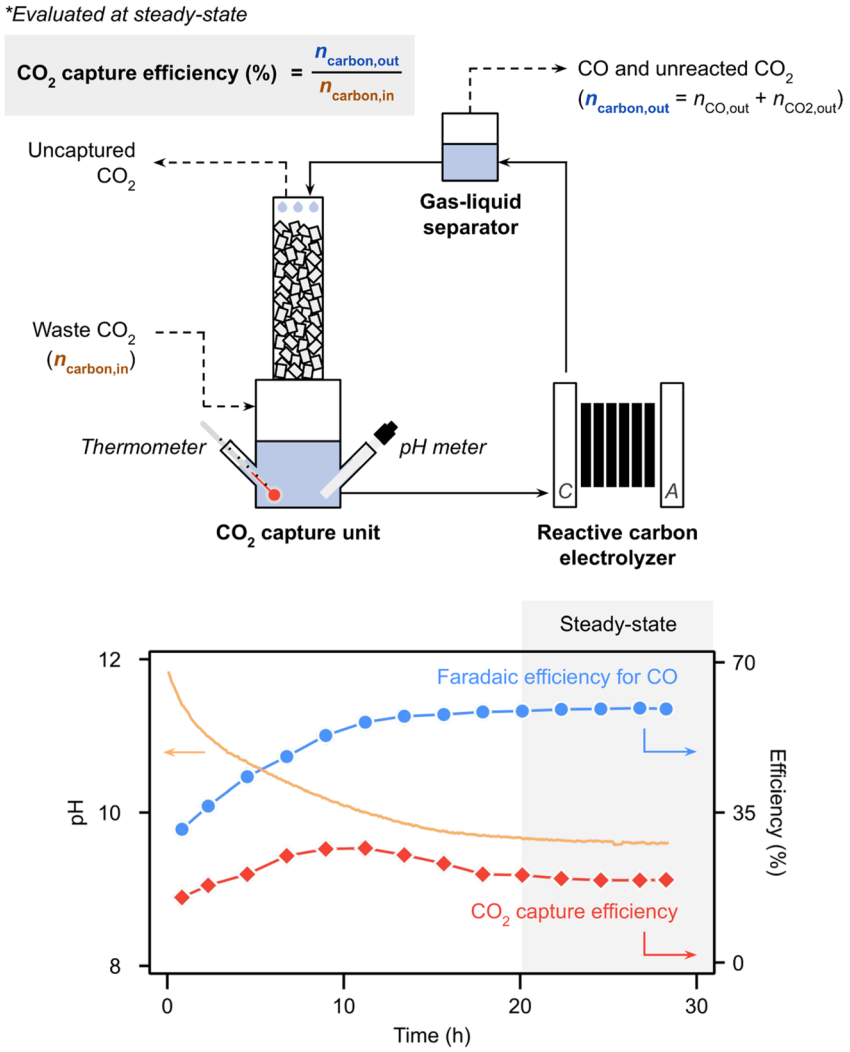

Fig. 2 A description of a representative reactive carbon capture experiment. The 1 M K_2CO_3 capture solution promoted with 0.1 M glycine is initially at a high pH (>12). At high pH, the CO_2 capture rate exceeds the CO_2 conversion rate, leading to a gradual pH decrease. Over time, the rates of CO_2 capture and conversion equilibrate, stabilizing the pH. Steady-state is defined as the period during which the pH remained constant. The CO_2 capture efficiency and FE_{CO} were evaluated under steady-state conditions. The CO_2 capture efficiency is calculated as the ratio of the molar flow rate of carbon exiting the gas–liquid separator ($n_{carbon,out}$) to the molar flow rate of carbon entering the CO_2 capture unit ($n_{carbon,in}$), where exiting carbon includes both CO and unreacted CO_2. Note: the initial measurements of CO_2 capture efficiency are unreliable for this experiment due to incomplete mixing, caused by the low flow rate of the reactive carbon solution (30 mL min^{-1}) relative to the reservoir volume (250 mL).

applied to the reactive carbon electrolyzer. We used an AI-driven approach to select the operating variables for each experiment. For simplicity, we fixed the CO_2 concentration in the simulated flue gas at 15%. We have previously established the effect of CO_2 concentration in flue gas on both CO_2 capture efficiency and FE_{CO}.[26] We maintained constant concentrations of 0.1 M glycine and 20 mM EDTA for all experiments. We used the "q-Noisy Expected Hyper volume Improvement" (qNEHVI)[28] algorithm to determine the experimental conditions most likely to maximize the objectives after each iteration. This algorithm is effective at handling data with significant noise (See SI Note 1 for a detailed justification of using qNEHVI).[29,32] We instructed the algorithm to optimize CO_2 capture efficiency and FE_{CO} over the 0–100% range. We assigned a 15% uncertainty to each objective to account for the variability in measurements. After each experiment, we used the measured FE_{CO} and CO_2 capture efficiency to update independent Gaussian process surrogate models, which were then used to evaluate candidate operating conditions across the defined parameter space. See SI Note 1 for a detailed description of the algorithm.

To initialize the optimizer, we selected eight starting sets of experimental conditions using the Latin hypercube sampling method,[33] a sampling strategy that spans a broad range of possibilities and provides the qNEHVI algorithm a diverse set of initial data points (Fig. 3; gray markers, and Table S1). We chose eight starting sets, equivalent to twice the number of manipulated variables, to balance computational efficiency with sufficient data to train the model effectively.[28] With the optimizer initialized, we performed additional experiments guided by the algorithm's recommendations. This allowed us to iteratively construct a Pareto front that mapped the combinations of experimental conditions that yield the highest CO_2 capture efficiency and FE_{CO} (Fig. 3; blue markers).

The Latin hypercube seed set affects the initial surrogate model and therefore can influence the early optimization trajectory. Although different Latin hypercube seeds could change the sequence of proposed experiments, the main trend identified using the optimizer was robust across the experimental campaign: high-performing conditions clustered at low simulated flue gas flow rate, high reactive carbon solution flow rate, and moderate current density.

After completing 21 AI-guided experiments, the optimization cycle concluded (Fig. S3) and discovered conditions that yielded an 83% CO_2 capture efficiency and a 42% FE_{CO} (Fig. 3 and Table S2). These optimized conditions correspond to a reactive carbon solution temperature of 25 °C, a solution flow rate of 100 mL min^{-1}, a flue gas flow rate of 35 sccm, and a current density of 234 mA cm^{-2}. The previous values were 30% CO_2 capture efficiency and 30% FE_{CO} for the previous best benchmark.[26] Importantly, the CO_2 capture efficiency approaches the industry benchmark of 90%.[34] Furthermore, a FE_{CO} of 42% produces syngas with an H_2 : CO molar ratio of 1.4, a ratio well-suited for synthesizing valuable hydrocarbons and oxygenates using the Fischer–Tropsch process.[35] The reactive carbon capture system demonstrated stable performance metrics over 80 hours of operation, with no noticeable decrease in either FE_{CO} or CO_2 capture efficiency (Fig. S4).

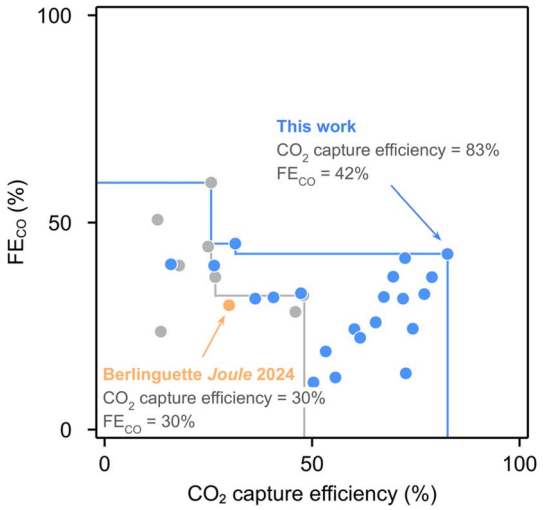

Fig. 3 Pareto front of artificial intelligence (AI)-guided reactive carbon capture experiments. The faradaic efficiencies for CO (FE_{CO}) and CO_2 capture efficiencies are shown for initialization experiments (gray markers) and AI-guided experiments (blue markers). The blue line represents the Pareto front identified in this study. The highest achieved values for FE_{CO} and CO_2 capture efficiency are 42% and 83%, respectively. These values represent 2.8-fold and 1.4-fold increases over the previous benchmarks for proof-of-concept reactive carbon capture, indicated by the orange marker.[26] The optimized conditions correspond to a reactive carbon solution temperature of 25 °C, a solution flow rate of 100 mL min^{-1}, a flue gas flow rate of 35 sccm, and a current density of 234 mA cm^{-2}.

We then evaluated how well the model's predictions matched the experimental results using a post hoc residual analysis (SI Note 2 and Table S3). The model agreed with the experiments in most cases, but one experiment (Exp. 19 in Table S3) yielded substantially lower CO_2 capture efficiency and FE_{CO} compared to experiments with similar conditions (Exp. 13 and 16 in Table S3). We retained this result because it reflects real-world variability and the system's sensitivity to small changes in operating conditions.

We also observed concurrent increases in other key performance indicators from these optimizations. Specifically, (i) the CO_2 utilization efficiency of the electrolyzer, defined as the fraction of *i*-CO_2 converted into CO (eqn (6)), and (ii) the overall CO_2 utilization efficiency, defined as the fraction of CO_2 introduced to the CO_2 capture unit that is converted to CO (eqn (7)). The CO_2 utilization efficiency of the electrolyzer was measured to be 80%, which is a substantial increase from 28% in our previous work.[26] Furthermore, we saw a significant improvement in the overall CO_2 utilization efficiency, with a measurement of 66% compared to a previous benchmark of 8%.[26] We attribute this improvement to the simultaneous increase in CO_2 capture efficiency of our system (from 30% to 83%, as previously discussed) and the CO_2 utilization efficiency of our electrolyzer.

$$\text{Electrolyzer } CO_2 \text{ utilization efficiency} = \frac{n_{CO,out}}{n_{carbon,out}} \quad (6)$$

$$\text{Overall } CO_2 \text{ utilization efficiency} = \frac{n_{CO,out}}{n_{carbon,in}} \quad (7)$$

Our statistical analysis, using multiple linear regression analysis with a two-tailed *t*-test at a 95% confidence level, shows that flue gas flow rate and current density significantly affect CO_2 capture efficiency and FE_{CO} (SI Note 3 and Fig. S5). Consistent with the optimization results, the highest-performing conditions occur at low flue gas flow rates and high liquid flow rates. The CO_2 capture efficiency increased as the flue gas flow rate decreased. We hypothesize that a lower flue gas flow rate into the CO_2 capture unit extends the residence time of CO_2, which increases CO_2 capture efficiency. The CO_2 capture efficiency increased with increasing current density, while FE_{CO} decreased with increasing current density. This trend aligns with the fact that higher current densities accelerate hydroxide generation (eqn (2)), leading to a faster recovery of the alkalinity of the reactive carbon solution. Furthermore, we have previously shown that FE_{CO} decreases with increasing current density.[17] Guided by these trade-offs, the optimizer converged toward conditions of low flue gas flow rate, high liquid flow rate, and moderate current density, balancing CO_2 capture efficiency and high FE_{CO}.

Techno-economic model and life cycle assessment

We then set out to determine the breakeven price for CO production from reactive carbon capture using the optimal CO_2 capture efficiency and FE_{CO} reported herein. We performed a discounted cash flow analysis to calculate the 20-year net present value. A detailed description of the techno-economic model is provided in SI Notes 4 and 5, along with Fig. S6 and Tables S4–S8. We determined the CO breakeven price using a net present value of zero. This analysis incorporates capital and operating costs for producing 100 tonnes of CO per day. We also accounted for the separation of unreacted CO_2 exiting the electrolyzer from the CO and H_2 products using a pressure swing adsorption unit ("separation unit"). We fixed the price of the H_2 product at \$2 per kg.[36] The cost of unreacted CO_2 exiting the electrolyzer was not considered in this analysis. However, this unreacted CO_2 could be sold, recycled, or sequestered. We assumed an electricity price of \$0.03 kW h^{-1}.[37] We calculated the breakeven price for CO production to be \$0.86 per kg. This estimate is lower than the breakeven price of \$0.97 per kg for CO production estimated by Resasco and coworkers. Their analysis considered a "sequential carbon capture and utilization" process, in which high-purity CO_2 is first released from the capture solution using heat, then upgraded to CO in a separate CO_2 electrolyzer.[38] Our estimate is higher than the \$0.44 per kg estimated by Jiao and coworkers for a similar sequential carbon capture and utilization approach.[39] The lower estimate by Jiao and coworkers is attributed to their assumption of a low CO_2 price. The market price for CO is widely accepted to be \$0.60 per kg.[39,40] We further project the breakeven price for CO production by reactive carbon capture could be decreased to a market-competitive \$0.61 per kg if the operating cell voltage of the electrolyzer is lowered to 3 V.

We performed a sensitivity analysis to evaluate how uncertainties in experimental performance propagate into the techno-economic model (Table S9). Key metrics such as FE_{CO}, CO_2 capture efficiency, electrolyzer CO_2 utilization efficiency, current density, and cell voltage were varied by ±10% from the optimized conditions (FE_{CO} = 42%; CO_2 capture efficiency = 83%; electrolyzer CO_2 utilization efficiency = 80%; current density = 234 mA cm^{-2}; and cell voltage = 4.8 V). FE_{CO} and cell voltage dominate cost sensitivity: varying FE_{CO} by ±10% changes the CO price by +8.1% to −8.1%, and varying cell voltage by ±10% changes CO price by +7.0% to −8.1%. CO_2 capture efficiency and electrolyzer CO_2 utilization efficiency have minimal impact within this range. When all parameters vary simultaneously, the CO price spans +22.1% to −18.6%.

We then calculated the carbon intensity of the optimized reactive carbon capture based on emissions associated with electricity generation (SI Note 6). We assumed that all unreacted CO_2 separated from the CO and H_2 product streams is either utilized, stored, or recycled, resulting in no direct process emissions. Electricity was assumed to be supplied by solar panels, consistent with our assumed electricity price of \$0.03 kW h^{-1}.[37] Modern solar power systems are reported to emit 0.043 kg CO_2 per kW h of electricity produced (*i.e.*, 0.043 kg_{CO_2} kW h^{-1}).[18] The reactive carbon capture process does not require any thermal energy input.

Under optimized operating conditions, the process emits 0.97 tonnes of CO_2 per tonne of CO produced (t_{CO_2} t_{CO}^{-1}). We project that this carbon intensity can be reduced to 0.61 t_{CO_2} t_{CO}^{-1} by lowering the cell voltage to 3 V, and further to 0.31 t_{CO_2} t_{CO}^{-1} if electricity is supplied by lower-carbon sources such as geothermal energy (0.022 kg_{CO_2} kW h^{-1}) at this reduced cell voltage.[18] These estimates fall within a reasonable range compared to literature values, which report a carbon intensity of 0.364 t_{CO_2} t_{syngas}^{-1} for a similar reactive carbon capture process. The same study reports a significantly higher carbon intensity of 1.393 t_{CO_2} t_{syngas}^{-1} for the sequential carbon capture and utilization, primarily due to the use of natural gas as the thermal energy source for releasing high-purity CO_2 from the capture solution.

Conclusions

Here, we used an AI-driven approach to optimize four key operating variables in the reactive carbon capture process. The AI-driven approach enabled us to achieve a CO_2 capture efficiency of 83% and a FE_{CO} of 42%. These values are substantial improvements over previous benchmarks of 30% CO_2 capture efficiency and 30% FE_{CO}. These results were achieved in just 21 AI-guided experiments, compared to an illustrative estimate of up to 9 million combinations required for a full grid search. A techno-economic analysis indicated that, with the CO_2 capture efficiency and FE_{CO} values, the breakeven price for CO production is \$0.86 per kg. Consequently, this work highlights a viable pathway for economical reactive carbon capture.

Author contributions

Conceptualization: C. P. B. and Y. K.; methodology: Y. K., M. M., and M. N.; investigation: Y. K., B. M. W. H., M. M., and M. N.; visualization: Y. K. and M. M.; funding acquisition: C. P. B.;

supervision: C. P. B.; writing – original draft: Y. K., M. M., G. V. C., and C. P. B.; writing – review and editing: all authors.

Conflicts of interest

This reactive carbon electrolyzer has been patented (*e.g.*, US Patent No. US12006580) and licensed, and CPB is a founder of a company commercializing the technology. The remaining authors declare no other competing interests.

Data availability

The optimization source code and complete experimental dataset are available in Zenodo at https://doi.org/10.5281/zenodo.20030202. The Zenodo record contains the file experiment_data.csv, which includes the full optimization dataset, as well as the optimization code, which includes the models and functions used for the closed-loop CO_2 capture and conversion optimization. The code is also openly available on GitHub repository code of berlinguette/ada under the tagged release adaccr-v1.0 (https://github.com/berlinguette/ada/releases/tag/adaccr-v1.0). All materials specific to this study are available in the directory "2025_12_Artificial intelligence-driven optimization of closed-loop CO_2 capture and conversion." The file "experiment_data.csv" contains the complete optimization dataset, while the "optimization_code/" folder includes all routines and models used for the closed-loop CO_2 capture and conversion optimization.

All data supporting the findings of this study are available within the article, its supplementary information (SI), and the Zenodo record. Ref. 41–55 are cited in the SI. Supplementary information is available. See DOI: https://doi.org/10.1039/d5dd00585j.

Acknowledgements

The authors are grateful to the Natural Sciences and Engineering Research Council of Canada (RGPIN-2024-06486; ALLRP-592435-2023), Canada Foundation for Innovation (229288), Canadian Institute for Advanced Research (BSE-BERL-162173), Canada Research Chairs, and TotalEnergies E&P Research & Technology USA LLC (an affiliate of TotalEnergies SE, France) for financial support. This research was undertaken thanks in part to funding provided to the University of Toronto's Acceleration Consortium from the Canada First Research Excellence Fund (CFREF-2022-00042).

References

1 G. T. Rochelle, Amine scrubbing for CO2 capture, *Science*, 2009, **325**(5948), 1652–1654.
2 D. W. Keith, Why capture CO2 from the atmosphere?, *Science*, 2009, **325**(5948), 1654–1655.
3 K. Sumida, D. L. Rogow, J. A. Mason, T. M. McDonald, E. D. Bloch, Z. R. Herm, *et al.*, Carbon dioxide capture in metal-organic frameworks, *Chem. Rev.*, 2012, **112**(2), 724–781.
4 H. Furukawa, K. E. Cordova, M. O'Keeffe and O. M. Yaghi, The chemistry and applications of metal-organic frameworks, *Science*, 2013, **341**(6149), 1230444.
5 D. W. Keith, G. Holmes, D. Angelo and K. Heidel, A Process for Capturing CO2 from the Atmosphere, *Joule*, 2018, **2**(8), 1573–1594.
6 S. Jin, M. Wu, R. G. Gordon, M. J. Aziz and D. G. Kwabi, pH swing cycle for CO2 capture electrochemically driven through proton-coupled electron transfer, *Energy Environ. Sci.*, 2020, **13**(10), 3706–3722.
7 I. Sullivan, A. Goryachev, I. A. Digdaya, X. Li, H. A. Atwater, D. A. Vermaas, *et al.*, Coupling electrochemical CO2 conversion with CO2 capture, *Nat. Catal.*, 2021, **4**(11), 952–958.
8 D. M. Weekes, D. A. Salvatore, A. Reyes, A. Huang and C. P. Berlinguette, Electrolytic CO2 Reduction in a Flow Cell, *Acc. Chem. Res.*, 2018, **51**(4), 910–918.
9 P. De Luna, C. Hahn, D. Higgins, S. A. Jaffer, T. F. Jaramillo and E. H. Sargent, What would it take for renewably powered electrosynthesis to displace petrochemical processes?, *Science*, 2019, **364**(6438), eaav3506.
10 S. Ren, D. Joulié, D. Salvatore, K. Torbensen, M. Wang, M. Robert, *et al.*, Molecular electrocatalysts can mediate fast, selective CO2 reduction in a flow cell, *Science*, 2019, **365**(6451), 367–369.
11 D. Higgins, C. Hahn, C. Xiang, T. F. Jaramillo and A. Z. Weber, Gas-Diffusion Electrodes for Carbon Dioxide Reduction: A New Paradigm, *ACS Energy Lett.*, 2019, **4**(1), 317–324.
12 E. W. Lees, B. A. W. Mowbray, F. G. L. Parlane and C. P. Berlinguette, Gas diffusion electrodes and membranes for CO2 reduction electrolysers, *Nat. Rev. Mater.*, 2021, **17**, 1–10.
13 S. Ren, E. W. Lees, C. Hunt, A. Jewlal, Y. Kim, Z. Zhang, *et al.*, Catalyst aggregation matters for immobilized molecular CO2RR electrocatalysts, *J. Am. Chem. Soc.*, 2023, **145**(8), 4414–4420.
14 D. J. D. Pimlott, Y. Kim and C. P. Berlinguette, Reactive Carbon Capture Enables CO2 Electrolysis with Liquid Feedstocks, *Acc. Chem. Res.*, 2024, **57**(7), 1007–1018.
15 M. Namdari, Y. Kim, D. J. D. Pimlott, A. M. L. Jewlal and C. P. Berlinguette, Reactive carbon capture using electrochemical reactors, *Chem. Soc. Rev.*, 2025, **54**(2), 590–600.
16 T. Li, E. W. Lees, M. Goldman, D. A. Salvatore, D. M. Weekes and C. P. Berlinguette, Electrolytic Conversion of Bicarbonate into CO in a Flow Cell, *Joule*, 2019, **3**(6), 1487–1497.
17 Z. Zhang, E. W. Lees, F. Habibzadeh, D. A. Salvatore, S. Ren, G. L. Simpson, *et al.*, Porous metal electrodes enable efficient electrolysis of carbon capture solutions, *Energy Environ. Sci.*, 2022, **15**, 705–713.
18 S. Nicholson and G. Heath, *Life cycle emissions factors for electricity generation technologies [Internet]*. National Renewable Energy Laboratory - Data (NREL-DATA), Golden, CO (United States), 2021, https://www.osti.gov/biblio/1819907.

19 D. J. D. Pimlott, A. Jewlal, B. A. W. Mowbray and C. P. Berlinguette, Impurity-Resistant CO2 Reduction Using Reactive Carbon Solutions, *ACS Energy Lett.*, 2023, **8**(4), 1779–1784.
20 D. J. D. Pimlott, A. Jewlal, Y. Kim and C. P. Berlinguette, Oxygen-Resistant CO2 Reduction Enabled by Electrolysis of Liquid Feedstocks, *J. Am. Chem. Soc.*, 2023, **145**(48), 25933–25937.
21 B. A. Rosen, A. Salehi-Khojin, M. R. Thorson, W. Zhu, D. T. Whipple, P. J. A. Kenis, *et al.*, Ionic Liquid–Mediated Selective Conversion of CO2 to CO at Low Overpotentials, *Science*, 2011, **334**(6056), 643–644.
22 Y. C. Li, D. Zhou, Z. Yan, R. H. Gonçalves, D. A. Salvatore, C. P. Berlinguette, *et al.*, Electrolysis of CO2 to Syngas in Bipolar Membrane-Based Electrochemical Cells, *ACS Energy Lett.*, 2016, **1**(6), 1149–1153.
23 D. A. Vermaas and W. A. Smith, Synergistic Electrochemical CO2 Reduction and Water Oxidation with a Bipolar Membrane, *ACS Energy Lett.*, 2016, **1**(6), 1143–1148.
24 D. A. Salvatore, D. M. Weekes, J. He, K. E. Dettelbach, Y. C. Li, T. E. Mallouk, *et al.*, Electrolysis of Gaseous CO2 to CO in a Flow Cell with a Bipolar Membrane, *ACS Energy Lett.*, 2018, **3**(1), 149–154.
25 Y. Kim, E. W. Lees and C. P. Berlinguette, Permeability Matters When Reducing CO2 in an Electrochemical Flow Cell, *ACS Energy Lett.*, 2022, **7**(7), 2382–2387.
26 Y. Kim, E. W. Lees, C. Donde, A. M. L. Jewlal, C. E. B. Waizenegger, B. M. W. de Hepcée, *et al.*, Integrated CO2 capture and conversion to form syngas, *Joule*, 2024, **8**(11), 3106–3125.
27 Y. Kim, M. Namdari, A. M. L. Jewlal, Y. Chen, D. J. D. Pimlott, M. Stolar, *et al.*, Economic viability of integrated CO2 capture and conversion, *ACS Energy Lett.*, 2024, 403–409.
28 S. Daulton, M. Balandat and E. Bakshy, Parallel Bayesian optimization of multiple noisy objectives with expected hypervolume improvement, *arXiv*, 2021, preprint, arXiv:2105.08195, DOI: 10.48550/arXiv.2105.08195.
29 S. Daulton, M. Balandat and E. Bakshy, Differentiable Expected Hypervolume Improvement for parallel multi-objective Bayesian optimization, *arXiv*, 2020, preprint, arXiv:2006.05078, DOI: 10.48550/arXiv.2006.05078.
30 Z. Zhang, E. W. Lees, S. Ren, B. A. W. Mowbray, A. Huang and C. P. Berlinguette, Conversion of Reactive Carbon Solutions into CO at Low Voltage and High Carbon Efficiency, *ACS Cent. Sci.*, 2022, **8**(6), 749–755.
31 J. He, A. Huang, N. J. J. Johnson, K. E. Dettelbach, D. M. Weekes, Y. Cao, *et al.*, Stabilizing copper for CO2 reduction in low-grade electrolyte, *Inorg. Chem.*, 2018, **57**(23), 14624–14631.
32 M. Balandat, B. Karrer, D. R. Jiang, S. Daulton, B. Letham and A. G. Wilson, *et al.*, BoTorch: A framework for efficient Monte-Carlo Bayesian optimization, *arXiv*, 2019, preprint, arXiv:1910.06403, DOI: 10.48550/arXiv.1910.06403.
33 M. D. Shields and J. Zhang, *The generalization of Latin hypercube sampling*, *arXiv*, 2015, preprint, arXiv:1507.06716, DOI: 10.48550/arXiv.1507.06716.
34 S. Budinis, M. Fajardy and C. Greenfield, *Carbon Capture, Utilisation and Storage*, IEA, https://www.iea.org/energy-system/carbon-capture-utilisation-and-storage.
35 J. R. Rostrup-Nielsen, Syngas in perspective, *Catal. Today*, 2002, **71**(3), 243–247.
36 *Global Hydrogen Review 2024 [Internet]*, International Energy Agency, 2024 Oct, https://iea.blob.core.windows.net/assets/89c1e382-dc59-46ca-aa47-9f7d41531ab5/GlobalHydrogenReview2024.pdf.
37 N. M. Haegel, R. Margolis, T. Buonassisi, D. Feldman, A. Froitzheim, R. Garabedian, *et al.*, Terawatt-scale photovoltaics: Trajectories and challenges, *Science*, 2017, **356**(6334), 141–143.
38 S. C. da Cunha and J. Resasco, Insights from techno-economic analysis can guide the design of low-temperature CO2 electrolyzers toward industrial scaleup, *ACS Energy Lett.*, 2024, **9**(11), 5550–5561.
39 H. Shin, K. U. Hansen and F. Jiao, Techno-economic assessment of low-temperature carbon dioxide electrolysis, *Nat Sustainability*, 2021, **4**(10), 911–919.
40 M. Jouny, W. Luc and F. Jiao, General Techno-Economic Analysis of CO2 Electrolysis Systems, *Ind. Eng. Chem. Res.*, 2018, **57**(6), 2165–2177.
41 L. Bertuccioli, A. Chan, D. Hart, F. Lehner, B. Madden, E. Standen. Development of Water Electrolysis in the European Union. 2014, https://www.h2knowledgecentre.com/content/researchpaper1120.
42 Umicore [Internet]. [cited 2024 Aug 16]. Available from: https://pmm.umicore.com/en/.
43 C. Maxwell, *Cost Indices*, https://toweringskills.com/financial-analysis/cost-indices/.
44 D. Peterson, J. Vickers, D. DeSantis Hydrogen production cost from PEM electrolysis. 2020, https://www.hydrogen.energy.gov/docs/hydrogenprogramlibraries/pdfs/19009_h2_production_cost_pem_electrolysis_2019.pdf?Status=Master.
45 D. Eriksson, M. Poloczek. Scalable Constrained Bayesian Optimization, in *International Conference on Artificial Intelligence and Statistics*. PMLR; 2021. p. 730–738.
46 A. M. Schweidtmann, A. D. Clayton, N. Holmes, E. Bradford, R. A. Bourne and A. A. Lapkin, Machine learning meets continuous flow chemistry: Automated optimization towards the Pareto front of multiple objectives, *Chem. Eng. J.*, 2018, **352**, 277–282.
47 H. M. Almajed, R. Kas, P. Brimley, A. M. Crow, A. Somoza-Tornos, B. M. Hodge, *et al.*, Closing the Loop: Unexamined Performance Trade-Offs of Integrating Direct Air Capture with (Bi)carbonate Electrolysis, *ACS Energy Lett.*, 2024, **9**(5), 2472–2483.
48 H2A: Hydrogen Analysis Production Models[Internet]. [cited 2024 Jul 15]. Available from: https://www.nrel.gov/hydrogen/h2a-production-models.html.
49 G. Towler, R. Sinnott. *Chemical engineering design : principles, practice, and economics of plant and process design*. Elsevier; 2021.

50 G. Holmes and D. W. Keith, An air-liquid contactor for large-scale capture of CO2 from air, *Philos. Trans. A Math. Phys. Eng. Sci.*, 2012, **370**, 4380–4403.
51 R. Turton. *Analysis, synthesis, and design of chemical processes*. 5th edn. Boston: Prentice Hall; 2018.
52 B. R. W. Pinsent, L. Pearson and F. J. W. Roughton, The kinetics of combination of carbon dioxide with hydroxide ions, *Trans. Faraday Soc.*, 1956, **52**, 1512–1520.
53 S. Bishnoi and G. T. Rochelle, Absorption of carbon dioxide into aqueous piperazine: reaction kinetics, mass transfer and solubility, *Chem. Eng. Sci.*, 2000, **55**(22), 5531–5543.
54 M. Hilliard. A predictive thermodynamic model for an aqueous blend of potassium carbonate, piperazine, and monoethanolamine for carbon dioxide capture from flue gas. 2008 May 1; Available from: https://repositories.lib.utexas.edu/items/2dc5e2ab-73dd-48e4-9df8-d5872933e64f.
55 T. J. Edwards, G. Maurer, J. Newman and J. M. Prausnitz, Vapor-liquid equilibria in multicomponent aqueous solutions of volatile weak electrolytes, *AIChE J.*, 1978, **24**(6), 966–976.